Electronic Supplementary Information

General strategy for fabrication of N-doped carbon nanotube/reduced graphene oxide aerogels for dissipation and conversion of electromagnetic energy

Jia Xu,[†] Yanan Shi,[†] Xinci Zhang,[†] Haoran Yuan,[†] Bei Li,[†] Chunling Zhu,[,‡] Xitian Zhang,[#] Yujin Chen[*,†]*

† Key Laboratory of In-Fiber Integrated Optics, Ministry of Education, College of Physics and Optoelectronic Engineering, Harbin Engineering University, Harbin 150001, China

‡ College of Material Science and Chemical Engineering, Harbin Engineering University, Harbin 150001, China

Key Laboratory for Photonic and Electronic Bandgap Materials, Ministry of Education, and School of Physics and Electronic Engineering, Harbin Normal University, Harbin 150025, China

* Corresponding author.

E-mail addresses: zhuchunling@hrbeu.edu.cn (C. Zhu), chenyujin@hrbeu.edu.cn (Y. Chen)

Experiment section

Materials

Nickel acetate tetrahydrate ($Ni(Ac)_2•4H_2O$), cobalt acetate tetrahydrate ($Co(Ac)_2•4H_2O$) and dicyandiamide were purchased from Tianjin Guangfu Fine Chemical Research Institute (China). Polyvinyl alcohol (PVA, 1750 ± 50) were purchased from Shanghai Sinopharm Chemical Reagent Co., Ltd (China). Paraffin was purchased from Yuyang Wax Industry (China).

The synthesis of CoNi−NGA

Graphene oxide (GO) was fabricated by the modified Hummers method using the graphite powders as starting material. 80 mg of GO was dispersed in 10 mL water to form the homogeneous brown dispersion in an ultrasonic bath for 1 h, which was marked as solution A. 64 mg $Ni(Ac)_2•4H_2O$ and 62 mg $Co(Ac)_2•4H_2O$ were dissolved in 2.5 mL PVA solution (16 mg mL^{-1}), which was marked as solution B. The A and B solutions were mixed by shaking violent and dispersed to form the homogeneous GO–PVA/$Ni(Ac)_2$–$Co(Ac)_2$ hydrogel. After the freeze-dried process for 72 h, the CoNi/PVA-GO xerogel was obtained. Then, the dicyandiamide (DCD) and CoNi/PVA-GO precursor with a weight ratio of 30:1 were preheated to 400 °C for 2 h, and to 800 °C with a ramping rate of 5 °C min^{-1} for 2 h under a flow of Ar. Finally, CoNi−NGA was obtained.

To control the NCNT concentration in the CoNi−NGA, the weight ratio of DCD/CoNi/PVA-GO precursor were adjusted to be 5:1, 10:1, 20:1 and 40:1. The corresponding final samples were named as CoNi−NGA-5, CoNi−NGA-10, CoNi−NGA-20 and CoNi−NGA-40, respectively.

The synthesis of Ni−NGA

Ni/PVA-GO was synthesized by a similar procedure, except for replacing $Ni(Ac)_2•4H_2O$ and $Co(Ac)_2•4H_2O$ with 128 mg $Ni(Ac)_2•4H_2O$. Ni−NGA was obtained by the same annealling process.

The synthesis of Co−NGA

Co/PVA-GO was synthesized by a similar procedure, except for replacing $Ni(Ac)_2•4H_2O$ and $Co(Ac)_2•4H_2O$ with 124 mg $Co(Ac)_2•4H_2O$. Co−NGA was obtained by the same annealling process.

The synthesis of CoNi−NGA−2 and CoNi−NGA−3

Besides, CoNi−NGA−2 and CoNi−NGA−3 with the molar ratio of Co^{2+} and Ni^{2+} is 1:2 and 2:1, respectively, were synthesized by the same processing method.

The synthesis of CoNi−NGA−700 and CoNi−NGA−900

As a contrast, the CoNi/PVA−GO was pyrolyzed in 700 and 900 °C for 2 h with a ramp rate of 5 °C min^{-1},

and products marked as CoNi−NGA−700 and CoNi−NGA−900, respectively.

The synthesis of FeCo−NGA

FeCo−NGA was synthesized by a similar procedure with CoNi−NGA, except for replacing $Ni(Ac)_2$•$4H_2O$ with 68 mg $FeCl_3$•$6H_2O$.

Characterizations

The structure and morphology of the prepared materials were characterized by X-ray diffraction (XRD, Rigaku D/max-2600/PC with Cu Kα radiation, λ=1.5418Å), Raman spectroscopy (Lab RAMA ramis, Horiba Jobin Yvon), Brunauer-Emmett-Teller (BET) surface area and pore volume (Quantachrome Instruments NOVA4000), scanning electron microscopy (SEM, Hitachi SU70), transmission electron microscopy (TEM, JEM-2010, JEOL), X-ray photoelectron spectroscopy (PHI 5700 ESCA System, Mg Kα radiation) and all XPS data were referenced to the C 1s = 284.6 eV. The magnetic property of aerogels samples were measured by a vibrating sample magnetometer (VSM; Lakeshore 7410) at room temperature. Inductively coupled plasma–optical emission spectrometry (ICP–OES) measurements were conducted on iCAP 6000 Series spectrometer for metal elemental analysis.

Electromagnetic parameter measurements

To investigate the microwave absorption performance, the reflection loss curves were measured with an Anritsu MS4644A Vectorstar vector network analyzer within a coaxial reflection/transmission anechoic chamber in the frequency range of 2–18 GHz. All aerogels were uniformly dispersed into the paraffin matrix. The samples pressed into to coaxial rings with the inner diameter 7.00 mm, the outer diameter 3.04 mm and the thickness 3.00 mm.

Calculation for electromagnetic absorbing performance

The reflection loss of EM wave. The reflection loss (R_L) can be calculated utilizing the complex permittivity (ε_r) and complex permeability (μ_r) by the following two equations:

$$R_L(\mathrm{dB}) = 20\log\frac{|Z_{in} - Z_0|}{|Z_{in} + Z_0|} \quad (1)$$

$$Z_{in} = Z_0(\mu_r/\varepsilon_r)^{1/2}\tanh[j(2\pi fd/c)(\mu_r/\varepsilon_r)^{1/2}] \quad (2)$$

where Z_0 is the impedance of free space, Z_{in} is the input impedance of the absorber, f is the frequency of microwaves, d is the thickness of the absorber, and c is the velocity of electromagnetic waves in free space, respectively.

The eddy current loss. The eddy current effect can be calculated by the following formulas:

$$\mu'' = 2\pi\mu_0(\mu')^2\sigma d^2 f/3 \quad (3)$$

$$C_0 = 2\pi\mu_0\sigma d^2/3 = \mu''(\mu')^{-2} f^{-1} \quad (4)$$

where μ_0 means the permeability of vacuum. If the eddy current effect occurs in magnetic absorbers, the C_0 will be a constant.

The conduction loss and polarization loss. The dielectric loss (ε'') of the EMW absorption materials can be dissected to the conduction loss (ε_c'') and polarization loss (ε_p''). According to Debye theory, the ε'' is defined as follow:

$$\varepsilon'' = \varepsilon_p'' + \varepsilon_c'' = \frac{\varepsilon_s - \varepsilon_\infty}{1 + \omega^2\tau^2}\omega\tau + \frac{\sigma}{\omega\varepsilon_0} \quad (5)$$

$$\varepsilon_p'' = \frac{\varepsilon_s - \varepsilon_\infty}{1 + \omega^2\tau^2}\omega\tau \quad (6)$$

$$\varepsilon_c'' = \frac{\sigma}{\omega\varepsilon_0} \quad (7)$$

where, ε_∞ is the relative dielectric permittivity at the high frequency limit, ε_s is the static permittivity, ω is the angular frequency, τ is the relaxation time for polarization, σ is the electrical conductivity, ε_0 is the dielectric constant in vacuum.

Cole–Cole semicircle. Debye relaxation expression as follow:

$$[\varepsilon' - (\varepsilon_s + \varepsilon_\infty)/2]^2 + (\varepsilon'')^2 = [(\varepsilon_s - \varepsilon_\infty)/2]^2 \quad (8)$$

The ε' versus ε'' plots would be a single semicircle, which is usually defined as the Cole–Cole semicircle.

The attenuation constant. The attenuation constant can be obtained by

$$\alpha = \frac{\sqrt{2\mu'\varepsilon'}\pi f}{c}\sqrt{\frac{\mu''\varepsilon''}{\mu'\varepsilon'} - 1 + \sqrt{\left(\frac{\mu''\varepsilon''}{\mu'\varepsilon'}\right)^2 + \left(\frac{\varepsilon''}{\varepsilon'}\right)^2 + \left(\frac{\mu''}{\mu'}\right)^2 + 1}} \quad (9)$$

The impedance coefficient. The impedance coefficient can be estimated by

$$M_z = \frac{2Z_{in}'}{|Z_{in}|^2 + 1} \quad (10)$$

where Z'_{in} represents the real parts of normalized input impedance.

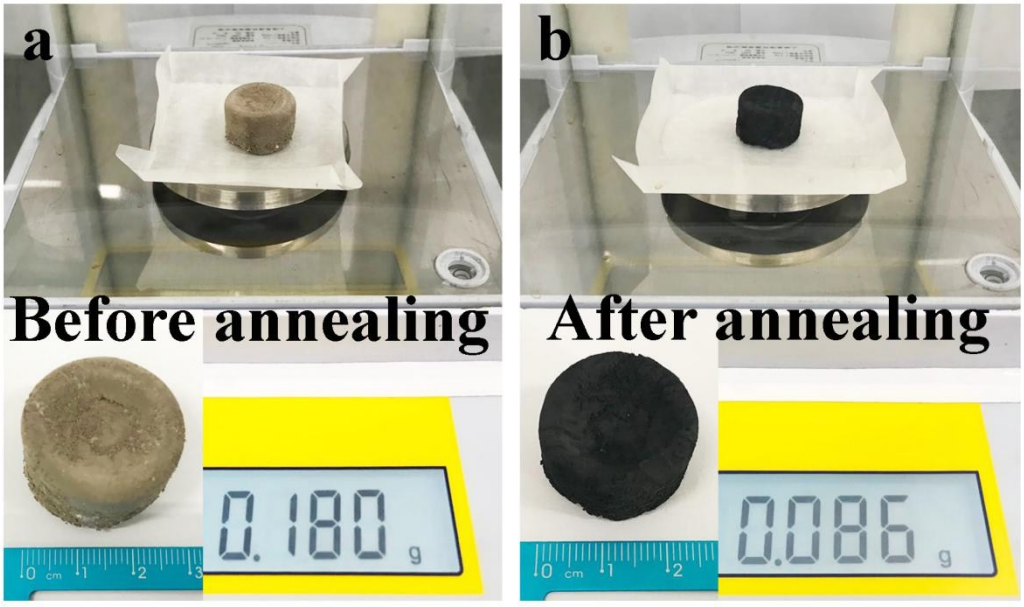

Fig. S1 The digital photograph of (a) CoNi/PVA−GO and (b) CoNi−NGA.

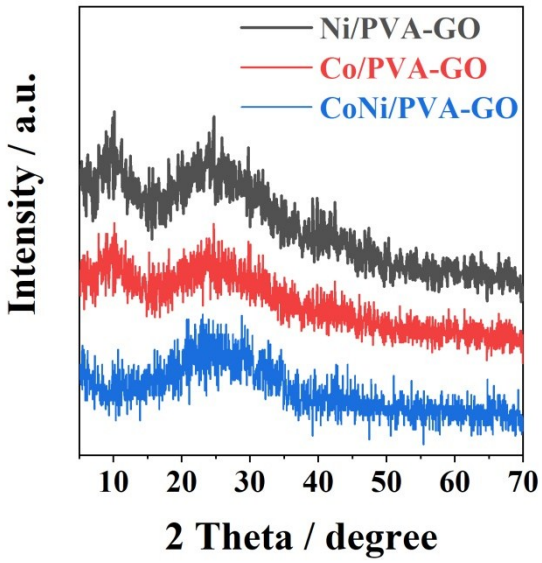

Fig. S2 XRD patterns of Ni/PVA-GO, Co/PVA-GO and CoNi/PVA-GO.

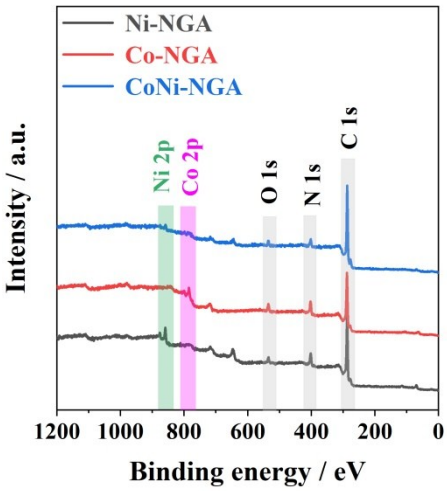

Fig. S3 XPS survey of all elements for Ni−NGA, Co−NGA and CoNi−NGA.

Note: The peaks around 720 eV can be assigned to Ag, Fe or Sn elements. The Ag, Fe or Sn elements come from impurity of analytical reagent such as metal precursors. The peaks around 650 eV can be assigned to Mn element. The Mn element originates from the impurity left in the GO due to the usage of $KMnO_4$ during fabrication of rGO. However, the contents of these impurities were greatly lower than those of Co and Ni, and thus they had little effect on the EM wave absorption property.

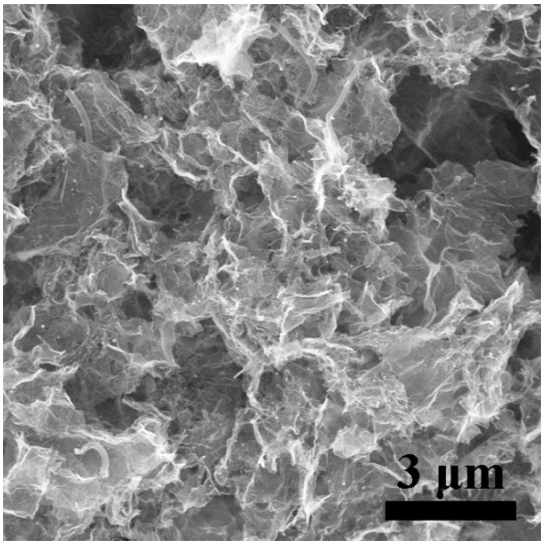

Fig. S4 SEM image of CoNi−NGA.

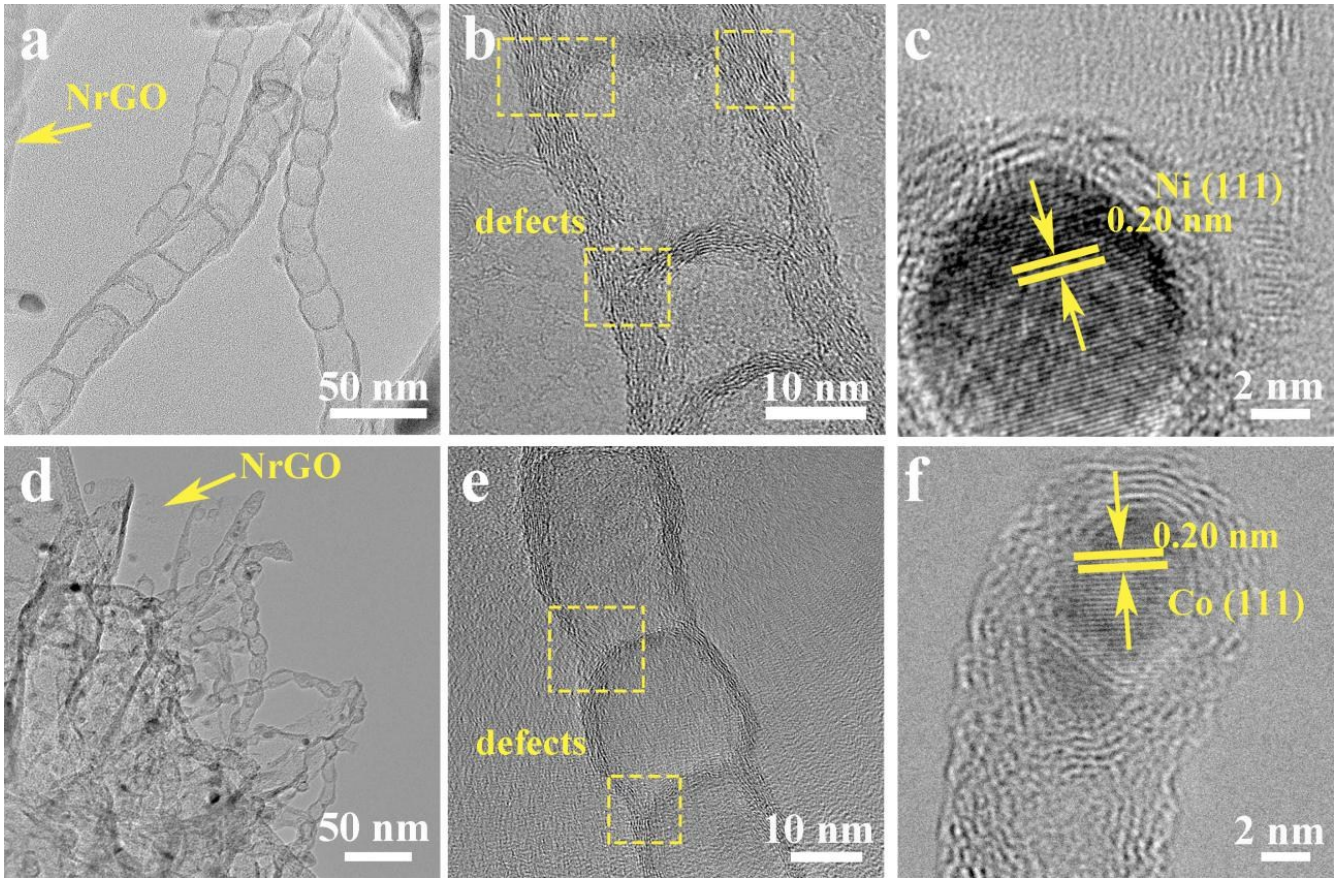

Fig. S5 (a, b) TEM images and (c) HRTEM image of Ni−NGA. (d, e) TEM images and (f) HRTEM image of Co−NGA.

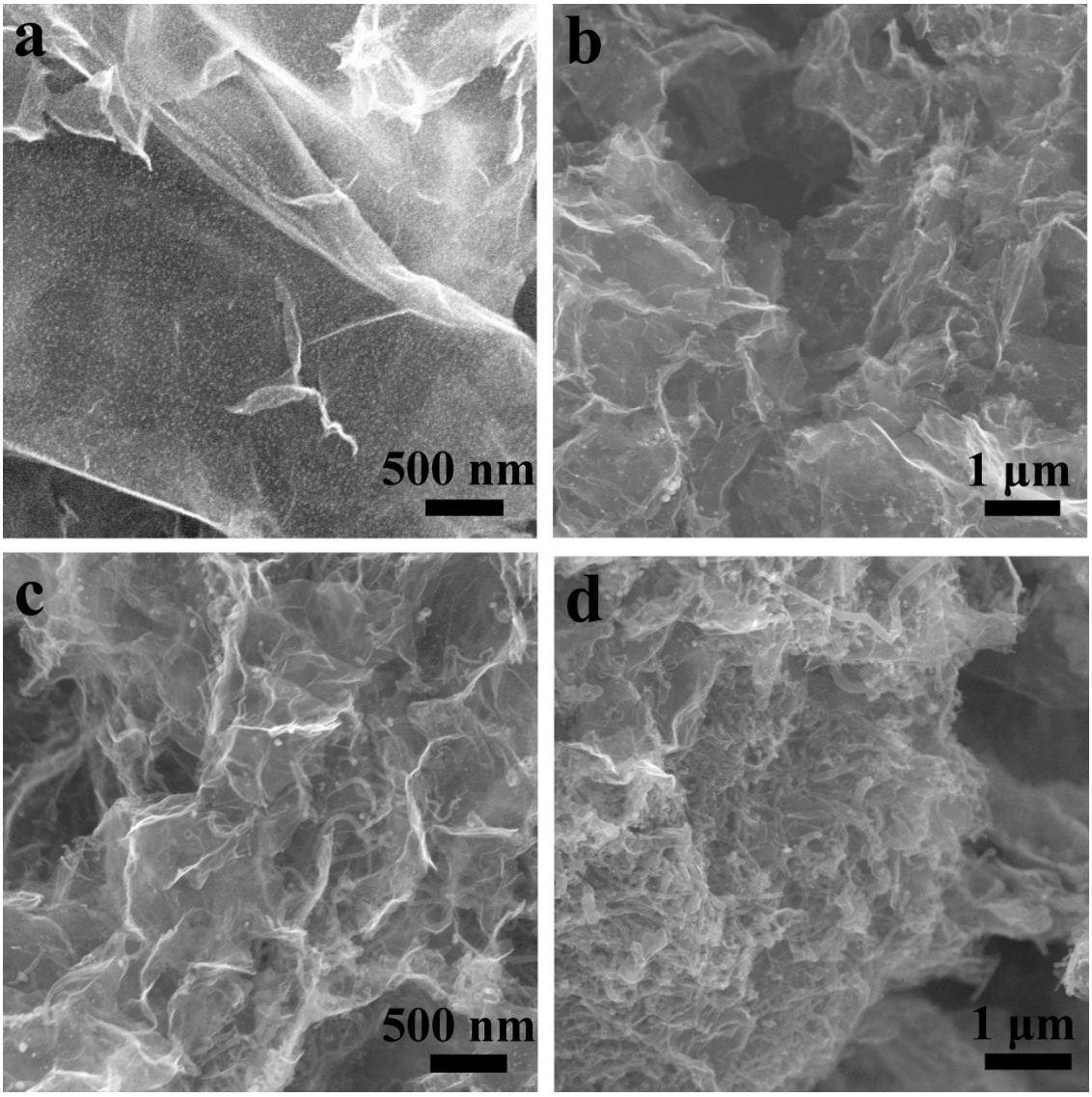

Fig. S6 SEM images of (a) CoNi−NGA−5, (b) CoNi−NGA−10, (c) CoNi−NGA−20 and (d) CoNi−NGA−40.

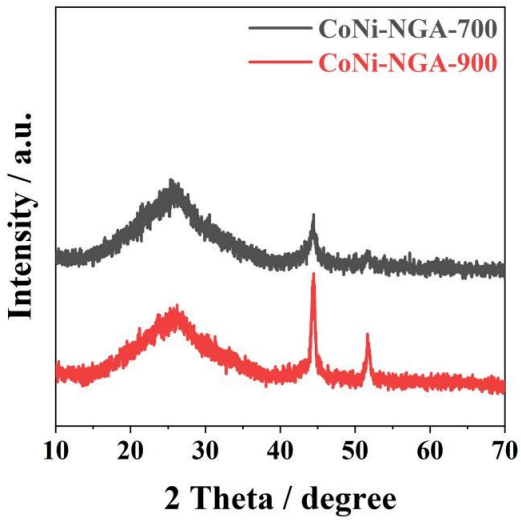

Fig. S7 XRD patterns of CoNi−NGA−700 and CoNi−NGA−900.

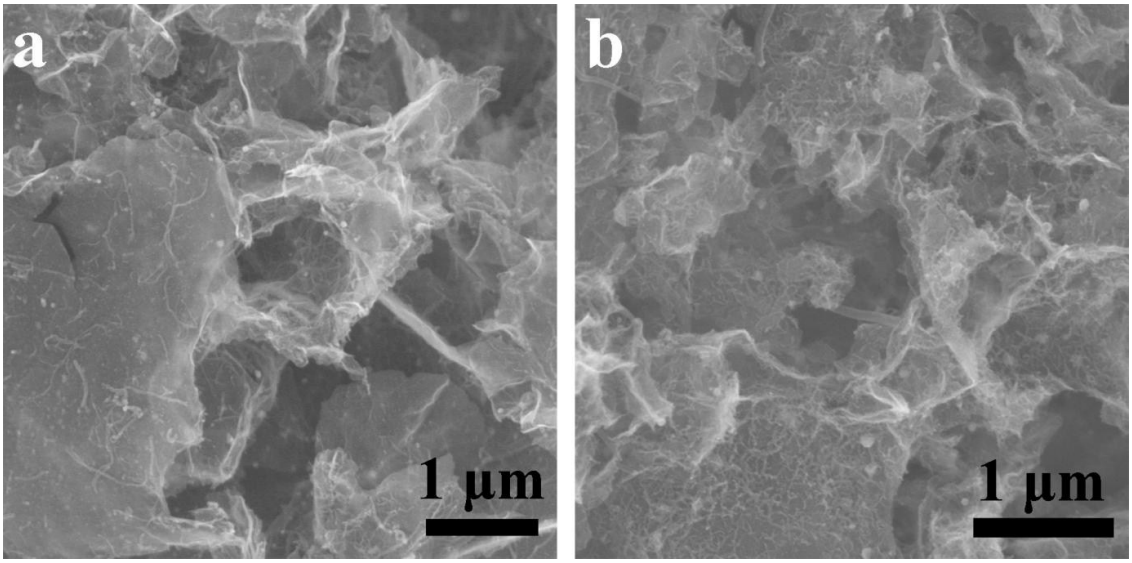

Fig. S8 SEM images of (a) CoNi−NGA−700 and (b) CoNi−NGA−900.

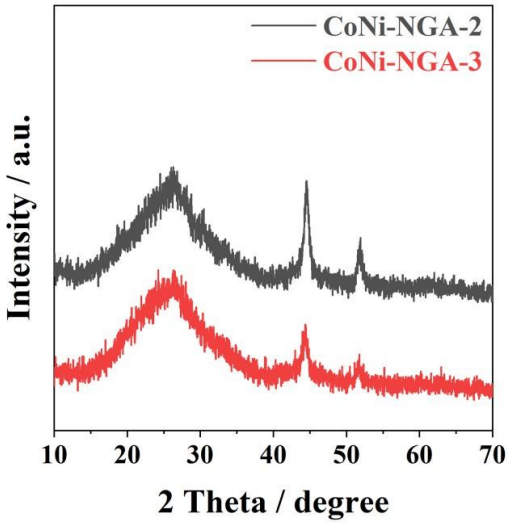

Fig. S9 XRD patterns of CoNi−NGA−2 and CoNi−NGA−3.

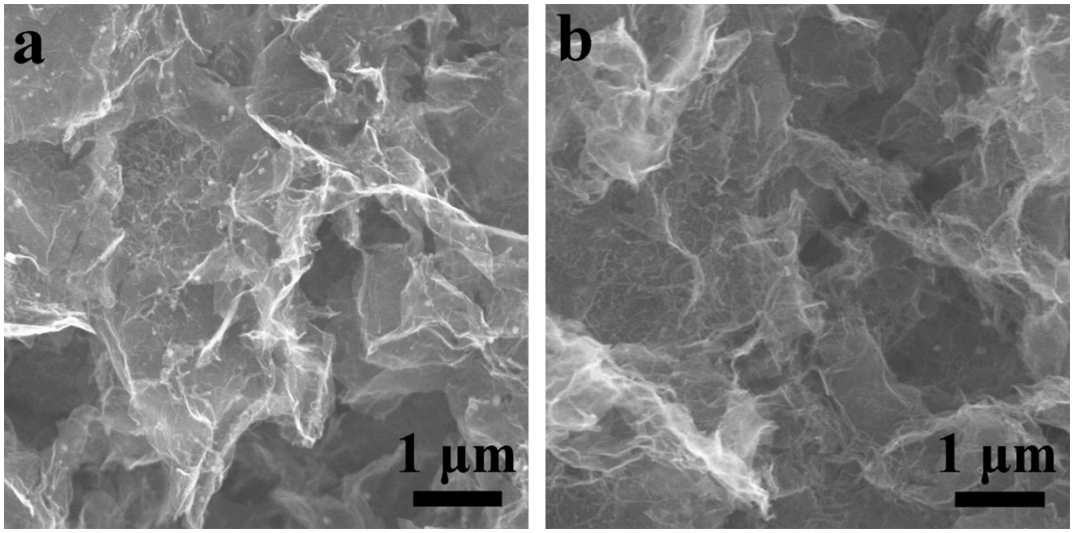

Fig. S10 SEM images of (a) CoNi−NGA−2 and (b) CoNi−NGA−3.

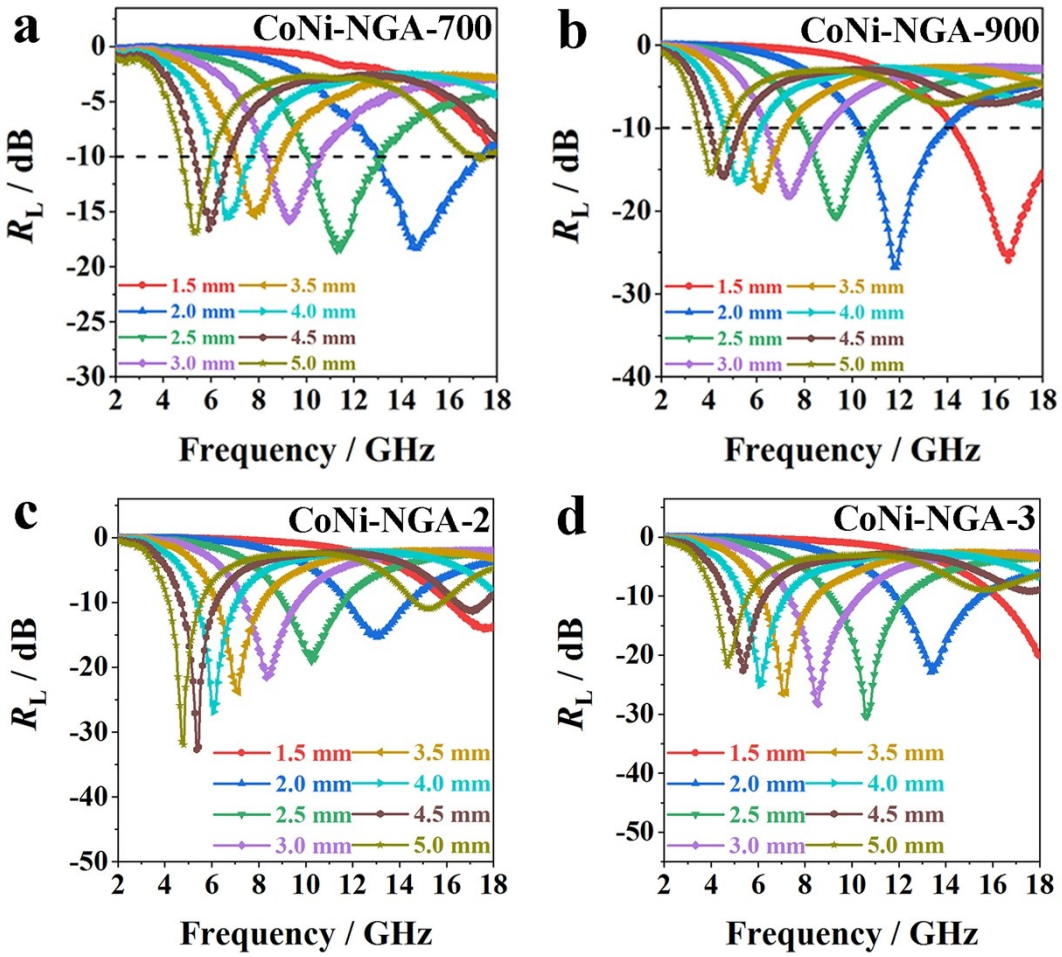

Fig. S11 The R_L–f curves of (a) CoNi−NGA−700, (b) CoNi−NGA−900, (c) CoNi−NGA−2 and (d) CoNi−NGA−3.

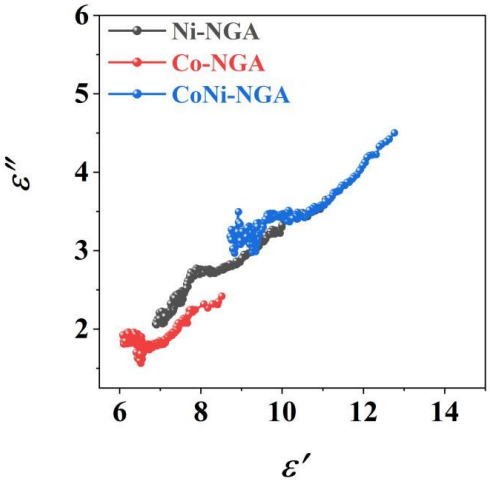

Fig. S12 Cole-Cole plots of Ni−NGA, Co−NGA and CoNi−NGA.

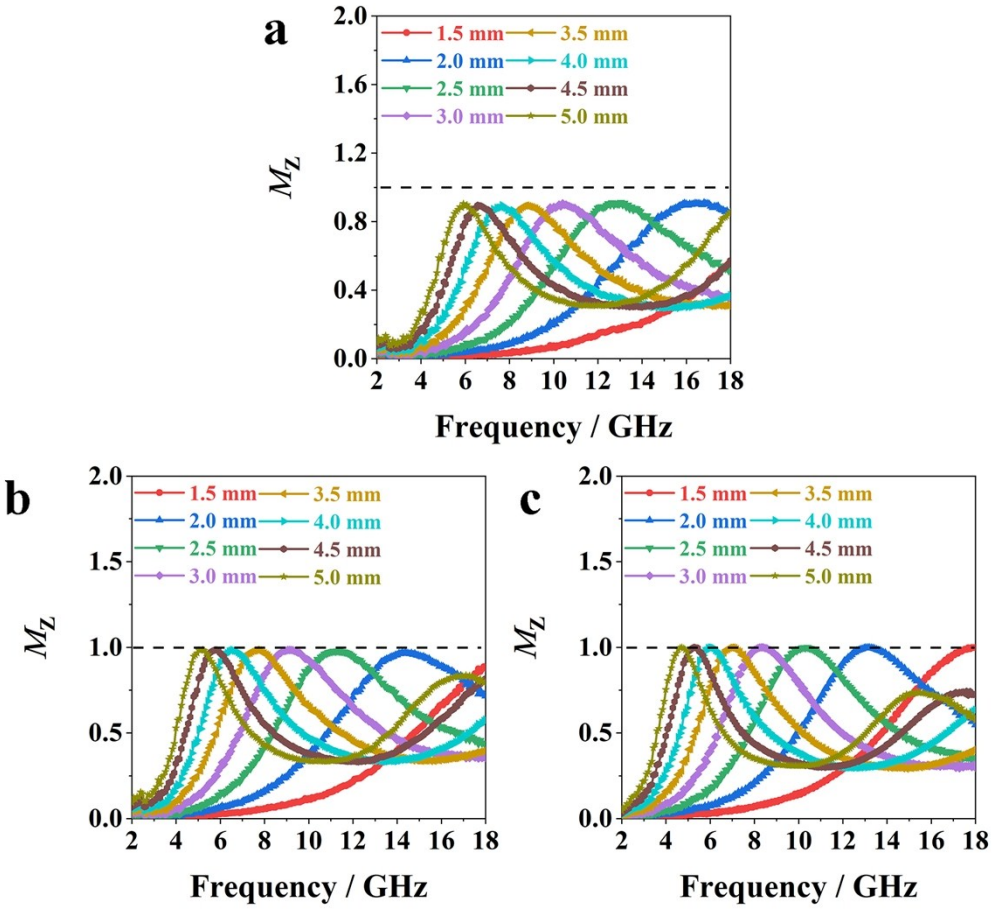

Fig. S13 M_Z–f curves of (a) Ni−NGA, (b) Co−NGA and (c) CoNi−NGA.

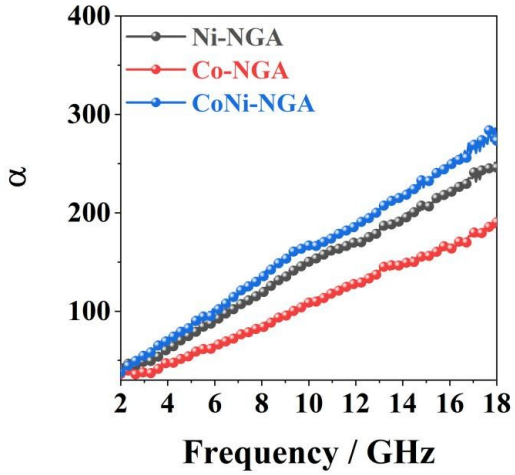

Fig. S14 *α–f* polts of Ni−NGA, Co−NGA and CoNi−NGA.

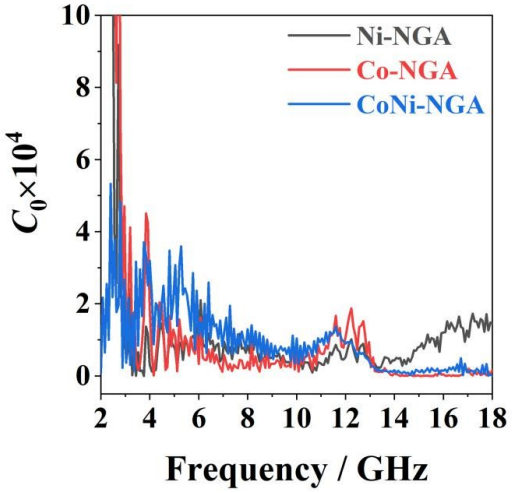

Fig. S15 C_0–*f* plots of Ni−NGA, Co−NGA and CoNi−NGA.

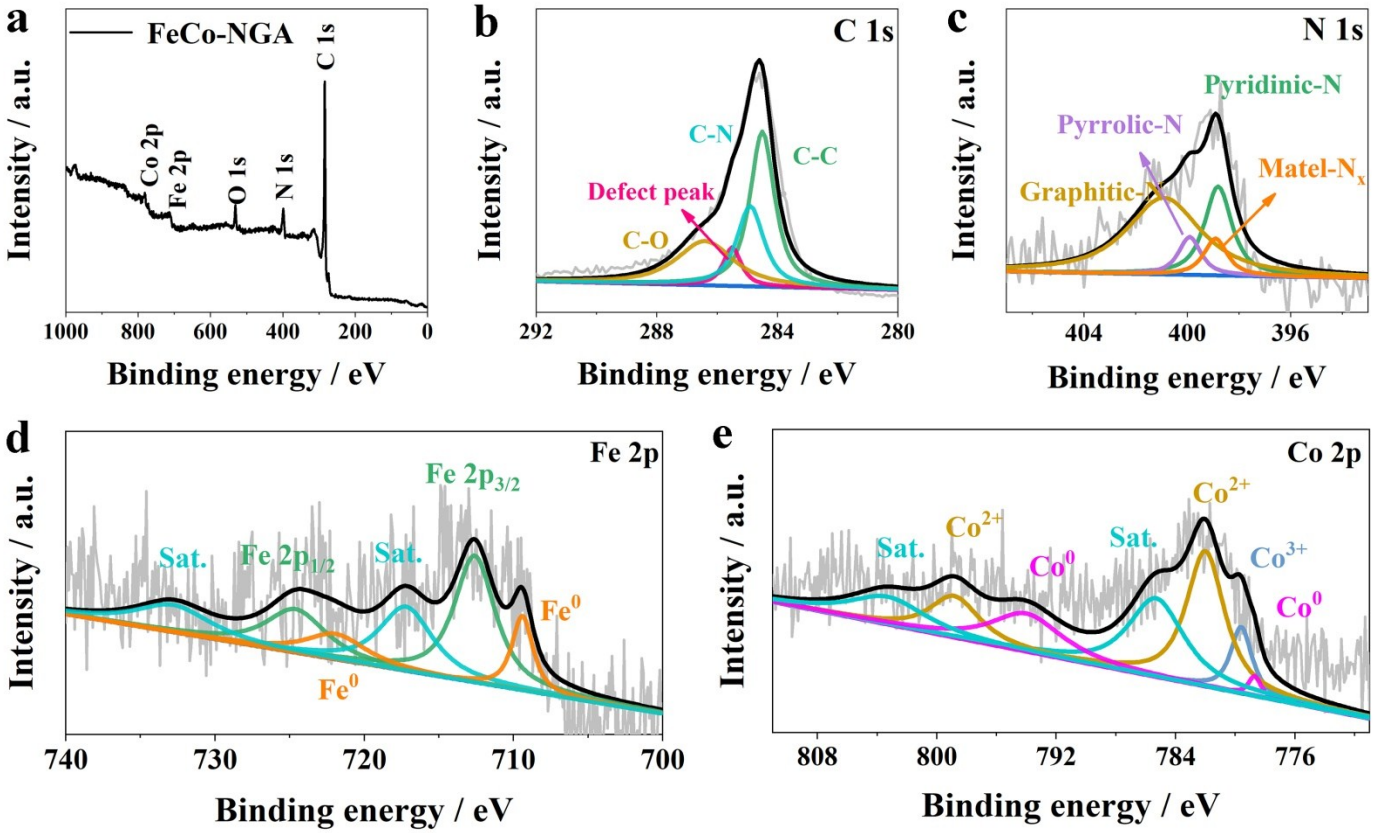

Fig. S16 (a) XPS survey of all elements for FeCo−NGA. (b) C 1s, (c) N 1s, (d) Fe 2p and (e) Co 2p XPS spectra of FeCo−NGA.

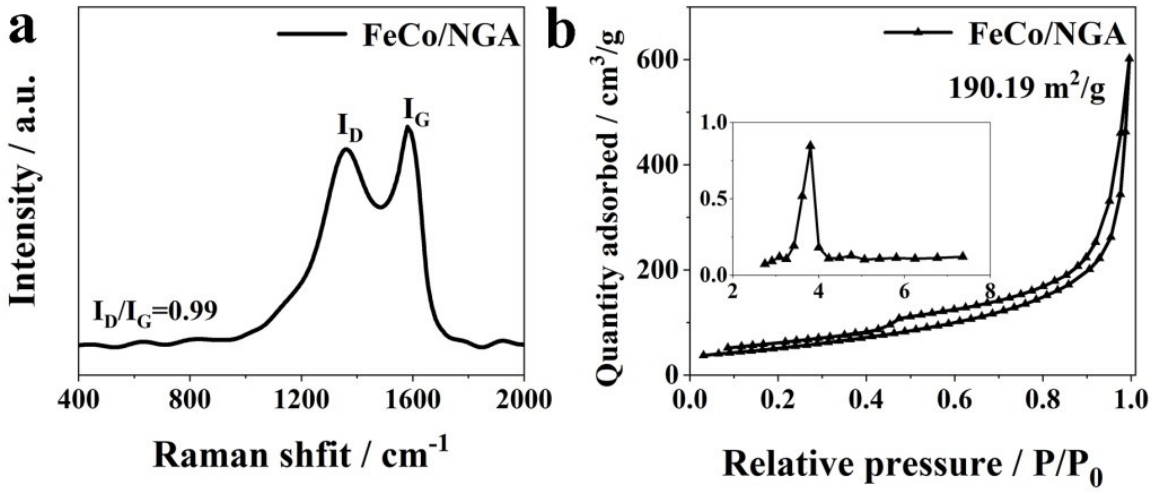

Fig. S17 (a) Raman and (b) nitrogen adsorption/desorption isotherms (pore size distribution in insert) of FeCo−NGA.

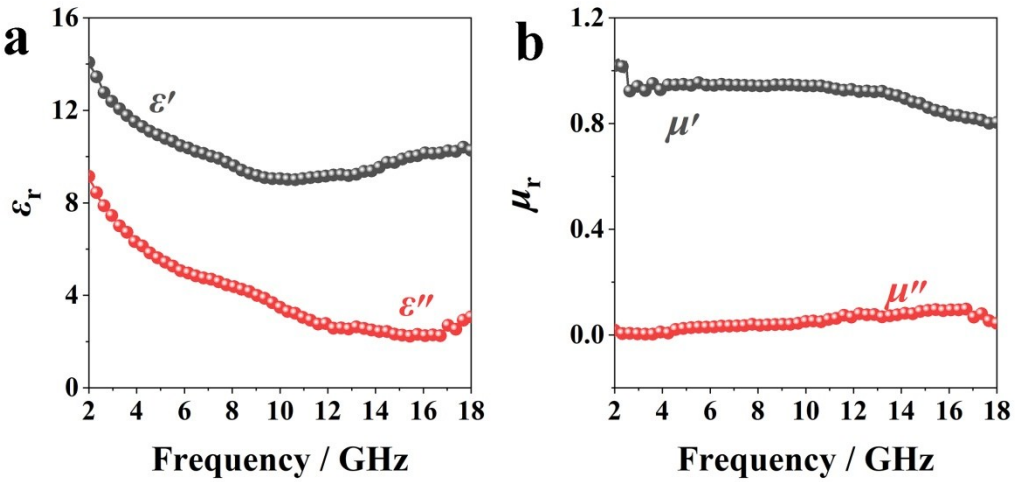

Fig. S18 (a) ε_r–f and (b) μ_r–f curves of FeCo−NGA.

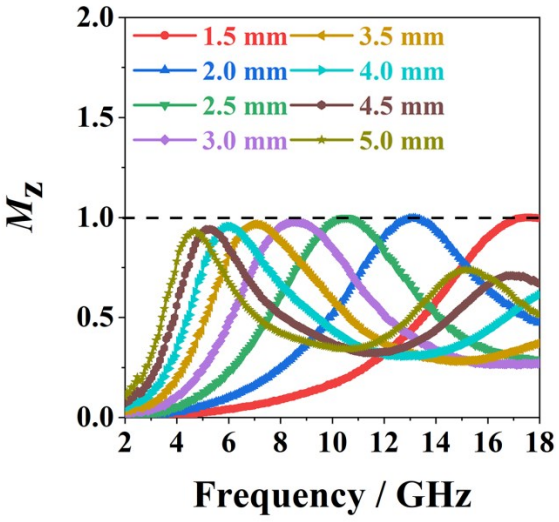

Fig. S19 M_z–f curves of FeCo−NGA.

Table S1 Elemental compositions of aerogels.

Samples	Elemental	ICP–OES	XPS (powder)
Ni−NGA	Ni	7.54 wt%	2.68 at%
	N	−	10.49 at%
Co−NGA	Co	7.43 wt%	2.51 at%
	N	−	11.16 at%
CoNi−NGA	Co	3.85 wt%	0.95 at%
	Ni	3.84 wt%	0.73 at%
	N	−	12.25 at%
CoNi−NGA-2	Co	2.51 wt%	−
	Ni	5.39 wt%	−
CoNi−NGA-3	Co	5.35 wt%	−
	Ni	2.61 wt%	−
FeCo−NGA	Fe	3.54 wt%	0.98 at%
	Co	3.82 wt%	1.07 at%
	N	-	11.81 at%.

Table S2 Comparison of EMW absorption property for absorbers previously reported.

Absorbers	$R_{L,min}$ (dB)	d (mm)	EAB_{10} (GHz)	Content (%)	Ref.
Co NPs/porous C	−30.31	3.0	4.93	25	1
CoNC/CNT	−44.6	1.5	4.5	15	2
Co−C/MWCNTs	−48.9	2.99	~3.7	15	3
Fe_3O_4/C Core−Shell Nanosheets	−43.95	4.3	3.0	21	4
$FeNi_3$/N-GN	−57.2	1.45	3.4	50	5
rGO/Ni	−39.03	2.0	4.3	50	6
NiS_2/NiS/rGO	−32.2	1.5	4.32	15	7
CoNi−NGA	-29.23	1.8	4.24	8	Herein
CoNi−NGA	-43.84	3.0	2.41	8	Herein
FeCo−NGA	-39.61	1.5	3.36	8	Herein

References

S1. H. Wang, L. Xiang, W. Wei, J. An, J. He, C. Gong, Y. Hou, *ACS Appl. Mater. Interfaces,* 2017, **9,** 42102-42110.

S2. X. Xu, F. Ran, H. Lai, Z. Cheng, T. Lv, L. Shao, Y. Liu, *ACS Appl. Mater. Interfaces,* 2019, **11,** 35999-36009.

S3. Y. Yin, X. Liu, X. Wei, Y. Li, X. Nie, R. Yu, J. Shui, *ACS Appl. Mater. Interfaces,* 2017, **9,** 30850-30861.

S4. Y. Liu, Y. Fu, L. Liu, W. Li, J. Guan, G. Tong, *ACS Appl. Mater. Interfaces* 2018, **10,** 16511-16520.

S5. J. Feng, Y. Zong, Y. Sun, Y. Zhang, X. Yang, G. Long, Y. Wang, X. Li, X. Zheng, *Chem. Eng. J.,* 2018, **345,** 441-451.

S6. W. Xu, G. Wang, P. Yin, *Carbon,* 2018, **139,** 759-767.

S7. M. Lu, N. Gao, X. Zhang, G. Wang, *RSC Advances,* 2019, **9,** 5550-5556.